# A mode-resolved continuum mechanics model of acoustic wave scattering from embedded cylinders

**Vineet Unni**
Department of Mechanical Engineering
University of Delaware
Newark, DE 19716
Email: vineetu@udel.edu

**Joseph P Feser***
Department of Mechanical Engineering
University of Delaware
Newark, DE 19716
Email: jpfeser@udel.edu

**ABSTRACT**

*In this paper, we use continuum mechanics to develop an analytic treatment of elastic wave scattering from an embedded cylinder and show that a classic treatise on the subject contains important errors for oblique angles of incidence, which we correct. We also develop missing equations for the scattering cross section at oblique angles and study the sensitivity of the scattering cross section as a function of elastodynamic contrast mechanisms. We find that in the Mie scattering regime for oblique angles of incidence, both elastic and density contrast are important mechanisms by which scattering can be controlled, but that their effects can offset one another, similar to the theory of reflection at flat interfaces. In comparison, we find that in the Rayleigh scattering regime elastic and density contrast are always complimentary toward increasing scattering cross section, but for sufficiently high density contrast, the scattering cross section for incident compressional and y-transverse modes is nearly independent of elastic contrast. The solution developed captures the scattering physics for all possible incident elastic wave orientations, polarizations and wavelengths including the transition from Rayleigh to geometric scattering regimes, so long as the continuum approximation holds. The method could for example enable calculation of the thermal conductivity tensor from microscopic principles which requires knowledge of the scattering cross section spanning all possible incident elastic wave orientations and polarizations at thermally excited wavelengths.*

**Nomenclature**

$\hat{a}$ Incident wavevector directional unit vector
$a$ Radius of embedded cylinder [m]
$\phi_i$ Compression wave propagation angle [rad]. Subscript denotes Region 1 or 2.
$\psi_i$ Transverse wave propagation angle [rad]. Subscript denotes Region 1 or 2.
$\tilde{u}$ Total displacement field [m]
$t$ time [s]
$\rho$ Density [kg/m$^3$-s]
$\mu_i$ 1st Lamé constant [Pa], Subscript denotes Region 1 or 2.
$\lambda_i$ 2nd Lamé constant [Pa], Subscript denotes Region 1 or 2.
$C_{ij}$ Components of the linear elastic tensor ($i, j = 1-6$) [Pa]
$\tilde{U}$ Spatial portion of displacement field [m]
$\omega$ Wave frequency [rad/s]

*Address all correspondence to this author.

$u_0$ Displacement amplitude [m]

$\Phi_i$ Generating function for incident ($i = inc$) or scattered compressional spatial wave displacements in Region 1 ($i = 1$) or 2 ($i = 2$).

$\Theta_i$ Generating functions for incident ($i = inc$) or scattered y-transverse spatial wave displacements.

$\chi_i$ Generating functions for incident ($i = inc$) or scattered quasi z-transverse spatial wave displacements.

$k_i$ Wavenumber [$m^{-1}$]. Subscript denotes wavetype and medium: $i = 1$ (compressional in Region 1), $i = 2$ (compressional in Region 2), $i = \mathrm{I}$ (transverse in Region 1), $i = \mathrm{II}$ (transverse in Region 2), $i = S$ (transverse wave in a generic medium).

$k_i'$ Projection of $k_i$ onto the $x$ axis.

$K$ Amplitude of wavevector projected onto z-axis [$m^{-1}$].

$\tilde{L}_i$ Compressional spatial portion of wave displacement [m]. Subscript denotes incident ($i = inc$) or scattered wave components in the Region 1 ($i = 1$) or Region 2 ($i = 2$)

$\tilde{M}_i$ y-transverse spatial portion of wave displacement [m]. Subscript denotes incident ($i = inc$) or scattered wave components in either Region 1 ($i = 1$) or Region 2 ($i = 2$)

$\tilde{N}_i$ Quasi z-transverse spatial portion of wave displacement [m]. Subscript denotes incident ($i = inc$) or scattered wave components in either Region 1 ($i = 1$) or Region 2 ($i = 2$)

$c_i$ Speed of sound [m/s]. Subscript denotes wavetype and medium: $i = 1$ (compressional, Region 1), $i = 2$ (compressional, Region 2), $i = \mathrm{I}$ (transverse, Region 1), $i = \mathrm{II}$ (transverse, Region 2).

$x_i$ Non-dimensional wavenumber. Subscript denotes wavetype and medium: $i = 1$ (compressional, Region 1), $i = 2$ (compressional, Region 2), $i = \mathrm{I}$ (transverse, Region 1), $i = \mathrm{II}$ (transverse, Region 2).

$x_i'$ Non-dimensional projected wavenumber. Subscript denotes wavetype and medium: $i = 1$ (compressional, Region 1), $i = 2$ (compressional, Region 2), $i = \mathrm{I}$ (transverse, Region 1), $i = \mathrm{II}$ (transverse, Region 2).

$T_{ij}$ Spatial portion of the stress tensor [Pa]

$\beta_n$ Non-dimensional expansion coefficients for generation of incident waves

$A_n$ Non-dimensional expansion coefficients for $\tilde{L}_2$

$B_n$ Non-dimensional expansion coefficients for $\tilde{M}_2$

$C_n$ Non-dimensional expansion coefficients for $\tilde{N}_2$

$D_n$ Non-dimensional expansion coefficients for $\tilde{L}_1$

$E_n$ Non-dimensional expansion coefficients for $\tilde{M}_1$

$F_n$ Non-dimensional expansion coefficients for $\tilde{L}_1$

$\sigma_{ij}$ Stress tensor [Pa]

$F$ Time-averaged energy flow [W]

$W$ Time-averaged energy flux [$W/m^2$]

$P$ Time-averaged scattered energy flow [W]

$dA_i$ Differential area vector [$m^2$]

$Q$ Total scattering cross section [m]

$Q_{xy}$ Polarization resolved components of scattering cross section [m]. $x$ denotes incident wave polarization: compressional ($x = C$) or transverse ($x = S$). $y$ denotes scattered polarization: compressional ($x = C$), y-transverse ($x = S_y$), or quasi-z transverse ($x = S_z$).

$\gamma$ Scattering efficiency, non-dimensional

$\alpha$ Scattering efficiency scaling factor in Rayleigh regime.

## 1 INTRODUCTION

Continuum mechanics is capable of yielding exact solutions to elastic wave scattering from isolated embedded particles for simple geometries like cylinders and spheres, where the embedded scatterer conforms to the coordinate axes. Such solutions can give polarization-specific scattering cross sections, take into account all sources of elastodynamic scattering contrast, do not rely on perturbation theory, and give results for arbitrary wavevector. White has reported an approach to calculate the scattered wave displacements for obliquely incident elastic waves from 3 dimensional embedded cylinders [1], and has experimentally validated the model in 2D (i.e. for wavevectors perpendicular to a cylinder axis). However, we will demonstrate that there are important errors when applying the equations developed by White to oblique angles of incidence. In addition, this classic treatise is missing the necessary equations to calculate the scattering cross section at oblique angles of incidence.

The objective of this manuscript is to redevelop the equations governing the scattered field such that they are corrected, to provide additional equations which allow the calculation of scattering cross section at oblique angles of incidence, and to study the polarization-dependant sensitivity of the scattering cross section as a function of elastodynamic contrast mechanisms and angle of incidence.

## 2 PROBLEM DEFINITION

Consider the scattering of a plane compressional or shear wave of a single frequency obliquely incident on an infinitely long isotropically elastic cylindrical discontinuity (medium 2) embedded in a different isotropic elastic medium (medium 1). Figure 1 shows the orientation of the cylinder and the incident wave with coordinate axes. The incident wave approaches with propagation direction in the x-z plane, defined by a wavevector along unit vector $\hat{a}$ ,which has an oblique incidence relative to the x-y plane. The angle between $\hat{a}$ and the x-y plane is denoted by $\phi_2$, for incident compressional waves or by $\psi_2$ for shear waves. The incident wave encounters a cylindrical scattering medium with radius $a$ from the z-axis denoted as region 1. This both produces a scattered wave in medium 2 and excites an internal wave in region 1. The total wave displacement in region 2 is a superposition of the incident and scattered waves. For continuity, both the displacements and the traction must be continuous at the interface between regions 1 and 2. If both media are linearly elastic with isotropic elastic tensors, then the equations of motion inside each medium are

$$\rho\frac{\partial^2\tilde{u}}{\partial t^2} = (\lambda+2\mu)\nabla(\nabla\cdot\tilde{u}) - \mu(\nabla\times\nabla\times\tilde{u}) \tag{1}$$

Where $\rho$ is the density of the material, and $\lambda$ and $\mu$ are the Lamé constants. The Lamé constants are easily connected to the elastic constants: $C_{11} = \lambda+2\mu$ and $C_{44} = \mu$. Considering displacements that are temporally sinusoidal ($\tilde{u} = \tilde{U}(x,y,z)e^{-i\omega t}$), any spatial portion of the displacement field, $\tilde{U}(x,y,z)$, for which $\tilde{u}$ satisfies Eq. 1 can be expressed as the superposition of displacements derived from scalar functions ($\Phi$, $\Theta$, and $\chi$) which satisfy scalar Helmholtz equations. In particular (1) if $(\nabla^2+k^2)\Phi = 0$ then $\tilde{L} = \nabla\Phi$ is a solution representing a longitudinal wave, (2) if $(\nabla^2+{k_S}^2)\Theta = 0$ then $\tilde{M} = \nabla\times(\hat{z}\Theta)$ is a solution representing a transverse wave with displacements polarized along the $\hat{z}\times\hat{a}$ direction, which is coincident with $\hat{y}$ and thus referred to a y-transverse wave from here on. (3) if $(\nabla^2+{k_S}^2)\chi = 0$ then $\tilde{N} = (1/k_S)\nabla\times\nabla\times(\hat{z}\chi)$ is a transverse wave with displacements polarized along $\hat{z}\times\hat{a}\times\hat{a}$. These displacements are orthogonal to both $\tilde{L}$ and $\tilde{M}$-type waves and will be referred to as quasi-z transverse waves because the displacements are in the $\hat{z}$ direction for waves at $\psi_2 = 0$ (normal incidence).

### 2.1 Incident Wave Expressions

The spatial portion of displacement for an incident compressional plane wave is of the form

$$\tilde{L}_{inc} = \hat{a}u_0 e^{ik_2(x\cos\phi_2+z\sin\phi_2)} \tag{2}$$

which can be derived from the scalar potential $\Phi_{inc}$ as $\tilde{L}_{inc} = \nabla\Phi_{inc}$ where

$$\Phi_{inc} = \frac{u_0}{ik_2}e^{ik_2(x\cos\phi_2+z\sin\phi_2)} \tag{3}$$

where $k_2 = \omega/c_2$ and $c_2 = \sqrt{(\lambda_2+2\mu_2)/\rho_2}$ is the sound speed of the compressional wave through region 2. This can be expressed in cylindrical coordinates as

$$\Phi_{inc} = \frac{u_0}{ik_2}\sum_{n=0}^{\infty} e^{iKz}e_n(i)^n J_n({k_2}'r)\cos(n\theta) \tag{4}$$

where

$$e_n = \begin{cases} 1 & : \quad n=0 \\ 2 & : \quad n>0 \end{cases} \tag{5}$$

and $K \equiv k_2\sin(\phi_2)$, and ${k_2}' \equiv k_2\cos(\phi_2)$.

The displacements due to transverse incident plane waves can be derived from scalar potentials in a similar manner. The potential

$$\Theta_{inc} = \frac{u_0}{ik_{\mathrm{II}}}\sum_{n=0}^{\infty} e^{iKz}e_n(i)^n J_n({k_{\mathrm{II}}}'r)\cos(n\theta) \tag{6}$$

generates a plane y-transverse incident wave via the operation $\tilde{M}_{inc} = \nabla \times (\hat{z}\Theta_{inc})$. Note that throughout the paper we denote the properties of transverse waves using roman numeral subscripts (i.e. $k_{\mathrm{II}}$ refers to the wavevector of a transverse wave in region 2), whereas properties of compressive waves are referred to using arabic subscripts (i.e. $k_2$ refers to the wavevector of a compressive wave in region 2). Thus, $k_{\mathrm{II}} = \omega/c_{\mathrm{II}}$ and $c_{\mathrm{II}} = \sqrt{\mu_2/\rho_2}$ is the sound speed of a shear wave through region 2. The scalar potential

$$\chi_{inc} = -\frac{u_0}{k_{\mathrm{II}}} \sum_{n=0}^{\infty} e^{iKz} e_n (i)^n J_n(k_{\mathrm{II}}{}' r) \cos(n\theta) \tag{7}$$

generates a plane quasi-z-transverse incident wave with displacements along the direction $\hat{z} \times \hat{a} \times \hat{a}$ via the operation $\tilde{N}_{inc} = 1/k_{\mathrm{II}}[\nabla \times \nabla \times (\hat{z}\chi_{inc})]$.

Given the potential functions, both the spatial portions of the incident wave displacement and stress field can be calculated. In particular, the radial components of the stress tensor can be obtained in cylindrical coordinates from the displacements using

$$T_{rr} = \lambda(\nabla \cdot \tilde{U}) + 2\mu \frac{\partial U_r}{\partial r} \tag{8}$$

$$T_{r\theta} = \mu \left( r \frac{\partial}{\partial r} \left( \frac{U_\theta}{r} \right) + \frac{1}{r} \frac{\partial U_r}{\partial \theta} \right) \tag{9}$$

$$T_{rz} = \mu \left( \frac{\partial U_z}{\partial r} + \frac{\partial U_r}{\partial z} \right) \tag{10}$$

The calculated displacement and stress fields are given in Tables 2-4 for the three possible polarizations of incident waves. Table 1 gives the definition of $\beta_n$, used in Tables 2-4, for each of the three incident polarizations. In some cases, such as in the calculation of $T_{rr}$, writing the simplified expressions in Tables 2-4 requires use of the recurrence relations for Bessel functions to eliminate first order derivatives (see Eq. 9.1.27 in Ref. 2). For convenience we define several non-dimensional parameters in Eqs. 11-14, so that displacements and stresses may be written on a non-dimensional basis.

$$x_2 = k_2 r \tag{11}$$
$$x_2{}' = k_2 r \cos(\phi_2) \tag{12}$$
$$x_{\mathrm{II}} = k_{\mathrm{II}} r \tag{13}$$
$$x_{\mathrm{II}}{}' = k_{\mathrm{II}} r \cos(\psi_2) \tag{14}$$

### 2.2 Scattered Wave Expressions

The scattered wave displacement fields in both region 1 and region 2 can be constructed as the superposition of compressional and shear waves. In region 2, the displacement field can be expressed as

$$\tilde{U}_{\mathrm{scat},2} = \tilde{L}_2 + \tilde{M}_2 + \tilde{N}_2 \tag{15}$$

where

$$\tilde{L}_2 = \sum_{n=0} A_n (\nabla \Phi_n) \tag{16}$$

$$\tilde{M}_2 = \sum_{n=0} B_n (\nabla \times (\hat{z}\Theta_n)) \tag{17}$$

$$\tilde{N}_2 = 1/k_{\mathrm{II}} \sum_{n=0} C_n(\nabla \times \nabla \times (\hat{z}\chi_n)) \tag{18}$$

The permitted scalar functions $\Phi_n$, $\Theta_n$, and $\chi_n$ satisfy the scalar Helmholtz equation, and must be chosen to be compatible with the incident wavevector/polarization at the interface of the cylindrical discontinuity. In region 2, the relevant potentials are

$$\Phi_n(r,\theta,z) = e^{iKz} H_n(k_2 \cos(\phi_2) r) \begin{matrix}\cos(n\theta) \\ \sin(n\theta)\end{matrix} \tag{19}$$

$$\Theta_n(r,\theta,z) = e^{iKz} H_n(k_{\mathrm{II}} \cos(\psi_2) r) \begin{matrix}\sin(n\theta) \\ \cos(n\theta)\end{matrix} \tag{20}$$

$$\chi_n(r,\theta,z) = e^{iKz} H_n(k_{\mathrm{II}} \cos(\psi_2) r) \begin{matrix}\cos(n\theta) \\ \sin(n\theta)\end{matrix} \tag{21}$$

The choice of upper or lower trigonometric function depends on whether the incident wave is longitudinal (upper function) or transverse (lower function). The wavenumbers must be choosen to have the same frequency as the incident wave, $\omega = c_2 k_2 = c_{\mathrm{II}} k_{\mathrm{II}}$. In region 2, the Hankel function of the first kind, $H_n \equiv J_n + iY_n$, is chosen because it represents a traveling wave carrying energy away from the cylinder as opposed to $H_n^{(2)} \equiv J_n - iY_n$ which carries energy toward the cylinder, or $J_n$ and $Y_n$ which individually represent standing waves. Analogous arguments can be made to construct the scattered displacement field in region 1, however in region 1 the displacement field must be finite at the origin. The relevant expansion can be obtained using Eqs. 15-21, but with a different set of expansion coefficients, using Bessel functions of the first kind, and by using wavenumber/angles that correspond to region 1. These substitutions are summarized in Table 5 and yield the following generating potentials for region 1

$$\Phi_n(r,\theta,z) = e^{iKz} J_n(k_1 \cos(\phi_1) r) \begin{matrix}\cos(n\theta) \\ \sin(n\theta)\end{matrix} \tag{22}$$

$$\Theta_n(r,\theta,z) = e^{iKz} J_n(k_I \cos(\psi_1) r) \begin{matrix}\sin(n\theta) \\ \cos(n\theta)\end{matrix} \tag{23}$$

$$\chi_n(r,\theta,z) = e^{iKz} J_n(k_I \cos(\psi_1) r) \begin{matrix}\cos(n\theta) \\ \sin(n\theta)\end{matrix} \tag{24}$$

where again the wavenumbers are choosen to allow temporal phase-matching with the incident wave, so that the frequency, $\omega = c_1 k_1 = c_I k_I$. The values of $K = k_2 \sin(\phi_2) = k_{\mathrm{II}} \sin(\psi_2) = k_1 \sin(\phi_1) = k_I \sin(\psi_1)$ must be the same in Eqs. 19-24 in order for the spatial phase of waves to be matched at the interface of the cylinder, which gives rise to an elastic analog to Snell's law.

$$\frac{\sin\phi_1}{c_1} = \frac{\sin\psi_1}{c_{\mathrm{I}}} = \frac{\sin\phi_2}{c_2} = \frac{\sin\psi_2}{c_{\mathrm{II}}} \tag{25}$$

Thus, one uses the known angle of incidence (either $\phi_2$ or $\psi_2$) to calculate the the remaining three angles from Eqs. 25.

### 2.3 Matching Conditions

The displacement and stress tensor fields at the boundary of the cylinder must be continuous at the interface between region 1 and region 2. This gives the closure necessary to solve for the unknown expansion coefficients $A_n$, $B_n$, $C_n$, $D_n$, $E_n$, and $F_n$ defining the scattered waves. At each value $n$ of the summation ($n = 0, 1, 2, \cdots, \infty$), the matching conditions define a set of 6 linear algebraic equations to be solved. These can be summarized as

$$\begin{aligned}(U_i)^n_{L_2} + (U_i)^n_{M_2} + (U_i)^n_{N_2} + \cdots \\ -(U_i)^n_{L_1} - (U_i)^n_{M_1} - (U_i)^n_{N_1} = -(U_i)^n_{\text{inc}}\end{aligned} \tag{26}$$

and

$$\begin{aligned}(T_{ir})^n_{L_2} + (T_{ir})^n_{M_2} + (T_{ir})^n_{N_2} + \cdots \\ -(T_{ir})^n_{L_1} - (T_{ir})^n_{M_1} - (T_{ir})^n_{N_1} = -(T_{ir})^n_{\text{inc}}\end{aligned} \tag{27}$$

where in both Eq. 26 and 27 the index, $i = r$, $\theta$, or $z$ refers to the cylindrical directional component evaluated at the cylinder surface, and $n$ refers to the index of the summand (not an algebraic power). The displacement expressions for each term can be obtained by performing the operations in Eq. 16-18 on the potential functions 19-21. The resulting expressions for the displacements and stresses are given in Tables 6-8 for the scattered wave in region 2. To save space, the expressions associated with region 1 are not explicitly shown but are easily obtained by the substitutions in Table 5.

Importantly, a number of non-trivial discrepancies are found when the expressions in Tables 6-8 are compared with those given in Ref. 1 at non-zero angles of incidence. In particular, the expression given for $T_{rr}$ in Table I.A. of Ref. 1, as well as all six expressions associated with $C_n$ for the stress and displacement components in Table I.B. of that reference are given incorrectly. In spite of these errors, the expressions in Ref. 1 will still give correct results in the special case where the angle of incidence is zero. However, in the more general case of oblique incidence, the expressions in the current manuscript must be used.

## 3 CALCULATION OF SCATTERING CROSS SECTION

The expansion coefficients of the scattered waves $A_n$, $B_n$, $C_n$, $D_n$, $E_n$, and $F_n$, corresponding to any incident wave of arbitrary polarization and angle of incidence, can be determined by applying the matching conditions, Eqs. 26 and 27, separated for each index of the summand. However, the displacements/stresses of scattered fields are typically of less direct importance than the rate that energy is scattered from an embedded object. This is quantified through the scattering cross section, $Q$, defined as the rate at which energy is scattered from an embedded object, $P$, relative to the energy intensity propagated by the incident plane wave, $W$. For an embedded cylinder of infinite extent, the units for $P$ are given on a per unit length basis [W/m], and the units for $W$ are [W/m$^2$]; thus, for a cylinder $Q$ has units of meters [m]. Note that for a sphere, the units for $Q$ are different, [m$^2$], because then $P$ has units [W]. White has previously given expressions for the scattering cross section for a cylindrically embedded scatterer subject to an incident elastic wave at *normal* incidence[1]. Here we develop expressions for the more general case of oblique angles of incidence; these are required, for example, in applications such as calculating thermal transport properties due to phonon transport.

The time-averaged energy flow through a surface can be calculated from the time dependent displacements, $u_j(r,\theta,z,t)$, and stresses, $\sigma_{ij}(r,\theta,z,t)$, as

$$F = \left\langle \iint \left[ \sigma_{ij}(r,\theta,z,t) \cdot \frac{\partial u_j(r,\theta,z,t)}{\partial t} \right] \cdot dA_i \right\rangle_t \tag{28}$$

where the outer bracket denotes a time-average. Up until now displacement and stress have been treated as complex quantities, but for calculation of energy flow we are interested in real displacements leading to real stresses. To obtain results in their real form, complex conjugates of the solutions are added.

$$\sigma_{ij}(r,\theta,z,t) = \frac{1}{2}\left[ \left(T_{ij}e^{-i\omega t}\right) + \left(T_{ij}e^{-i\omega t}\right)^* \right] \tag{29}$$

$$u_j(r,\theta,z,t) = \frac{1}{2}\left[ \left(U_j e^{-i\omega t}\right) + \left(U_j e^{-i\omega t}\right)^* \right] \tag{30}$$

Carrying out the time-averaging operation gives an average energy flow

$$F = \frac{i\omega}{4} \iint [(T_{ij}^* U_j) - (T_{ij} U_j^*)] \cdot dA_i \tag{31}$$

The energy flux [W/m$^2$] carried by an incident plane wave, W, can be obtained from this by considering a planar area perpendicular to the direction of travel, in which case the incident power/area is just the prefactor and integrand of Eq. 31 projected onto the direction of travel.

$$W = \frac{i\omega}{4} \left[ (T_{ij}^* U_j) - (T_{ij} U_j^*) \right] \cdot \hat{a}_i \tag{32}$$

After some manipulation it can be shown that the energy flux for incident longitudinal and both transverse polarization are respectively given by

$$W_{long} = \frac{(\lambda_2 + 2\mu_2) {u_0}^2 k_2 \omega}{2} \tag{33}$$

$$W_{trans} = \frac{\mu_2 {u_0}^2 k_{II} \omega}{2} \tag{34}$$

Simple expressions for the scattered energy can be obtained by applying Eq. 31 on an imaginary cylinder of radius $b \gg a$. In that case the Hankel function takes on the limiting behavior [2]

$$H_n(x') \to \left( \frac{2}{\pi x'} \right)^{1/2} e^{i(x' - (n+1/2)\pi/2)}. \tag{35}$$

Using ${H_n}'(x') \to iH_n$ and ${H_n}''(x') \to -H_n$ and taking $b \to \infty$, gives the limiting behavior of wave energy carried by the L, M, N scattered waves as

$$P_L = \sum_{n=0}^{\infty} A_n A_n^* (2\mu_2 + \lambda_2) \left( \omega {k_2}^2 \right) \tag{36}$$

$$P_M = \sum_{n=0}^{\infty} B_n B_n^* \left( \mu \cos^2 \psi_2 \right) \left( \omega {k_{II}}^2 \right) \tag{37}$$

$$P_N = \sum_{n=0}^{\infty} C_n C_n^* (\mu \cos^2 \psi_2) \left( \omega k_{II}^2 \right) \tag{38}$$

Equations 36-38 are correct regardless of the polarization of incident wave. The scattering cross section for incident waves of type $i$ ($i$ =compressional ($C$), y-transverse ($S_y$) or quasi z-transverse ($S_z$)) into scattered waves of polarization j is then

$$Q_{ij} = P_j / W_i \tag{39}$$

For incident compression waves, these become

$$Q_{CC} = \frac{2}{k_2} \left( 2\|A_0\|^2 + \sum_{n=1}^{\infty} \|A_n\|^2 \right) \tag{40}$$

$$Q_{CS_y} = \frac{2}{k_2}\cos^2\psi_2 \left( 2\|B_0\|^2 + \sum_{n=1}^{\infty} \|B_n\|^2 \right) \tag{41}$$

$$Q_{CS_z} = \frac{2}{k_2}\cos^2\psi_2 \left( 2\|C_0\|^2 + \sum_{n=1}^{\infty} \|C_n\|^2 \right) \tag{42}$$

For incident shear waves of either polarization, these become

$$Q_{SC} = \frac{2}{k_{\mathrm{II}}} \left( 2\|A_0\|^2 + \sum_{n=1}^{\infty} \|A_n\|^2 \right) \tag{43}$$

$$Q_{SS_y} = \frac{2}{k_{\mathrm{II}}}\cos^2\psi_2 \left( 2\|B_0\|^2 + \sum_{n=1}^{\infty} \|B_n\|^2 \right) \tag{44}$$

$$Q_{SS_z} = \frac{2}{k_{\mathrm{II}}}\cos^2\psi_2 \left( 2\|C_0\|^2 + \sum_{n=1}^{\infty} \|C_n\|^2 \right) \tag{45}$$

In the case of obliquely incident shear waves, these expressions differ by a factor of $\cos^2(\psi_2)$ from those derived in Ref [1].

One other important physical aspect of calculating the scattering cross section is that due to Snell's Law (Eq. 25) some of the internal and external scattered modes may be evanescent waves. In the case of external scattered modes, this always happens when a transverse phonon with angle, $\psi > \sin^{-1}(c_T/c_L)$, is incident on a cylinder, producing an evanescent compressional mode. Evanescent modes can propagate no energy, yet in our formulation, the complex scattering coefficients, $\|A_n\|$, are generally still non-zero. This is because the expansion in Eqn. 35 is not the correct one for imaginary arguments and does not lead to the form given in Eq. 43, but rather $Q_{SC} = 0$ in that case. Therefore, we set $Q_{SC} = 0$ if $\mathrm{Im}(\phi) < 0$. Otherwise, the math in the preceding sections is correct and requires no special considerations to account for evanescent modes.

One final practical consideration is the number of terms to be evaluated. In principle, there are an infinite number of expansion coefficients, $A_n$, $B_n$, $C_n$, $D_n$, $E_n$, and $F_n$ since $n = 0, 1, 2, \cdots, \infty$. In the Rayleigh regime, usually only one or two of the lowest order terms are required for accurate results. However, in the geometric regime a large number of terms (often hundreds or thousands) are required for convergence and accuracy. Thus, we continue the calculation of expansion coefficients until a relative convergence tolerance for the scattering cross section is met. An open-source MATLAB implementation of the algorithm described in this manuscript has been made available via GitHub [3].

## 4 RESULTS AND DISCUSSION

Using the results of the previous section, we now investigate the scattering behavior of elastically embedded cylinders. In general the scattering cross section of an embedded cylinder is a function of up to 9 geometric and materials parameters:

$$Q = Q(a, k_2 \text{ or } k_{\mathrm{II}}, \phi_2 \text{ or } \psi_2, \lambda_1, \lambda_2, \rho_1, \rho_2, \mu_1, \mu_2) \tag{46}$$

Dimensional analysis can reduce the dependence to 6 non-dimensional variables. A convenient choice in the case of incident compressional waves is

$$\gamma = \gamma\left( k_2 a, \phi_2, \frac{\rho_1 - \rho_2}{\rho_2}, \frac{C_{11,1} - C_{11,2}}{C_{11,2}}, \frac{C_{44,1} - C_{44,2}}{C_{44,2}}, \frac{C_{11,2}}{C_{44,2}} \right). \tag{47}$$

A similarly convenient choice in the case of either polarization of incident transverse waves is

$$\gamma = \gamma\left(k_{\text{II}}a, \psi_2, \frac{\rho_1-\rho_2}{\rho_2}, \frac{C_{11,1}-C_{11,2}}{C_{11,2}}, \frac{C_{44,1}-C_{44,2}}{C_{44,2}}, \frac{C_{11,2}}{C_{44,2}}\right) \tag{48}$$

Here $\gamma \equiv \frac{Q}{2a}$ is the dimensionless scattering efficiency in 2D, representing the ratio of the scattering cross section relative to the cylinder's geometric cross section. $ka$ is called the scattering parameter. The 3rd term is the fractional density contrast and the 4th and 5th terms are the fractional longitudinal and shear elastic contrast of the two media respectively. The final terms is the ratio of the longitudinal to shear elastic constants $C_{11}/C_{44} = (\lambda+2\mu)/\mu$; For group IV and III-V semiconductors this spans a small range ($1.8 < C_{11}/C_{44} < 2.2$ for Si, Ge, GaP, GaAs, InAs, GaSb, InSb, InP). However, most other classes of cubic materials have higher $C_{11}/C_{44}$, with some as high as 9 (PbTe = 8.2, PbSe = 7.8, Nb = 8.6). Thus, when embedding particles with similar crystal structure and bonding chemistry, $\Delta C_{11}/C_{11} \approx \Delta C_{44}/C_{44}$, but this is generally not true otherwise. At this point, we should caution that the model developed in the preceding sections is strictly valid only for isotropic media, which is not the case for single crystals regardless of whether they have cubic crystal structure. However, the degree of anisotropy is not large in many cubic crystals (in Si for example the longitudinal sound speed in the [111] direction differs from [100] by about 10%), so it is hoped that the insights from the present model will still prove useful. To understand some general predictions of the model, we will now explore the scattering efficiency, $\gamma$, for some illuminating cases.

In Figure 2, scattering efficiency for phonons at normal incidence angle ($\psi_2 = 0$) is plotted for a $NiSi_2$ cylindrical discontinuity embedded in a $Si_{0.5}Ge_{0.5}$ matrix for size parameters ranging from the Rayleigh regime up to the geometric regime. The properties for these materials are given in Table 9. Some basic features are evident: (1) in the Rayleigh regime, scattering efficiency scales as $\gamma \sim (ka)^3$. Note that this is a different behavior than scattering from embedded spheres, where $\gamma_{sph} \sim (ka)^4$ (2) In the geometric regime, $\gamma$ oscillates about 2. (3) In the intermediate regime, Mie oscillations exist and these may persist for several orders of magnitude before and after $ka = 1$.

Figure 3 shows the scattering efficiency as a function of angle-of-incidence for low and high scattering parameter, and shows how the polarization makeup of the scattered wave changes with angle. Intuitively, based on geometric thinking, one might expect that scattering would be weaker for waves traveling parallel to the cylinder axis. While this intuition is confirmed in the geometric limit, it fails for long wavelength compressional waves which are strongly scattered into transverse waves even for parallel travel; in fact, in the Rayleigh regime compressional waves traveling parallel to the cylinder scatter more strongly than waves with normal incidence. Similar behavior is not observed for incident transverse waves, in part because compressional scattered modes are evanescent and carry no energy, while according to Snell's law, transverse waves scattering into transverse waves would carry energy along the axis of the cylinder. Thus no energy is scattered away from the cylinder for transverse waves coincident with the cylinder axis for any wavelength.

The limits of continuum theory as applied to scattering of thermal wavelength vibrations (i.e. phonons) warrant further discussion. Kakodkar [4] has recently compared the exact continuum model developed in this manuscript to an atomistically resolved computational model of phonon scattering for embedded cylinders with diameters between 2nm-9nm and for incident phonon wavelengths spanning the entire Brillouin zone. Kakodkar found excellent agreement between continuum and atomistically resolved theory for acoustic phonons in the first quarter of the Brillouin zone, which in the case of Ge embedded in Si was sufficient to capture the first Mie scattering oscillation in the toughest case of 2nm cylinder diameters or about 8 atoms wide [4]. However, we should note that in weaker scatterers, the first peak in the Mie oscillations generally occurs at higher wavenumber (see the longitudinal case in Fig. 2, for example), in which case the continuum model will correctly predict the lull before the first Mie peak, but will inaccurately describe physics near and above the first Mie oscillation. For wavevectors $k \gtrsim 0.25k_{max}$ continuum theory will fail, and in particular will miss important physical effects such as phonon dispersion, evanescent modes associated with phonon band gaps or maximum frequencies in the scattering medium, optical vibration modes, and the edge of the first Brillouin zone [4]. The current method also cannot model scattering of optical modes by nanostructures since optical modes are not predicted by continuum mechanics. However, the theory developed in the current manuscript may still of significant use for enabling thermal transport property estimation in fibrous nanocomposites because embedded nanostructures in thermal applications are typically designed to scatter long wavelength acoustic phonons, while other mechanisms such as phonon-phonon and point defect scattering are dominant at high wavevector and for optical modes. This warrants further investigation but is beyond the scope of this paper.

### 4.1 Contrast Mechanisms in the Mie and Rayleigh Regimes

The goal of this section is to determine which materials parameters or combinations have the greatest influence on the scattering efficiency. In the geometric limit, geometry alone determines the scattering efficiency, and thus the materials parameters are expected to have no influence. However, as shown in Fig. 2, transition to the geometric limit sometimes requires very large scattering parameter.

On the other hand, in the Mie and Rayleigh regimes the materials properties have great influence on the scattering cross section. Mie oscillations occur due to wave interference, the degree of which is determined both by geometry and

phase speed. The later depends on materials properties such as the speed of sound. In order to understand the transition from Rayleigh to geometric behavior, it is particularly important to understand how the first scattering efficiency peak (at low scattering parameter) is related to the matrix/particle materials properties. Figure 4 shows a psuedocolor image of the scattering efficiency as a function of both the relative elastic contrast and density contrast in the Mie regime, using either $k_2 a = 2$ or $k_{II} a = 2$ for longitudinal or transverse waves respectively. The evaluation is done at an angle of incidence of either $\phi_2 = 35°$(longitudinal) or $\psi_2 = 35°$ (transverse) rather than normal incidence because because elastic waves at this angle have the maximum differential contribution to thermal vibrational energy flow perpendicular to the axis of the cylinder in the BTE-derived thermal conductivity integral ($k = \int k(\phi) d\phi$ where $k(\phi) \sim \sin(\phi)\cos^2(\phi)$); thus, scattering effects at this angle are of great interest to heat transfer applications.

Figure 4 shows that the scattering efficiency is highly dependent on both density contrast, $\Delta\rho/\rho$ and elastic contrast $\Delta C_{11}/C_{11}$ or $\Delta C_{44}/C_{44}$ in the early Mie regime, and in particular, it shows that if the sound speed of the embedded cylinder is the same as that of the matrix, then the scattering efficiency is greatly suppressed, regardless of whether there is large density and/or elastic contrast. Fig. 4 also shows that large density contrast (in the absence of increased stiffness) is generally more effective at increasing scattering cross section than similar levels of elastic contrast. Alternatively, embedding a lower elastic constant material in the absence of density contrast is nearly as effective. Note that the scattering cross section does not monotonically rise with increasing contrast, though. This is in stark contrast to behavior in the Rayleigh regime ($ka \ll 1$).

In the Rayleigh regime, the scattering efficiency scales as $Q/2a = \alpha(ka)^3$. The scaling factor, $\alpha$, depends on elastodynamic contrast mechanisms as well as the incidence angle.

$$\alpha = \alpha\left(\phi_2, \frac{\rho_1 - \rho_2}{\rho_2}, \frac{C_{11,1} - C_{11,2}}{C_{11,2}}, \frac{C_{44,1} - C_{44,2}}{C_{44,2}}, \frac{C_{11,2}}{C_{44,2}}\right). \tag{49}$$

For a given matrix material (i.e. fixed $C_{11,2}/C_{44,2}$), we can then therefore more universally capture results in the Rayleigh regime by plotting $\alpha$. If there is no contrast (i.e. $\frac{C_{11,2}-C_{11,1}}{C_{11,2}} = \frac{C_{44,2}-C_{44,1}}{C_{44,2}} = \frac{\rho_2-\rho_1}{\rho_2} = 0$) then $Q$ must be zero, and since $Q \geq 0$, the function $\alpha$ must also be a local minimum.

Fig. 5 shows a contour plot of $\alpha$ as a function of elastic and density contrast for a group IV matrix material ($C_{11,2}/C_{44,2} = 2$) such as $Si_{1-x}Ge_x$ subject to obliquely incident waves ($\phi_2 = 35°$(longitudinal) or $\psi_2 = 35°$ (transverse)). In the Rayleigh limit, $\alpha$ and, by extension, the scattering cross section show sensitivity to both density and elastic contrast for weak levels of contrast. However, for longitudinal and y-transverse incidence polarizations, the scattering cross-section becomes nearly independent of elastic contrast once the density contrast is sufficiently large ($\Delta\rho/\rho_2 \gtrsim 1$); The scattering cross section of z-transverse polarization waves is co-dependent on density and elastic contrast over the entire range studied.

## 5 Conclusions

In summary, we have developed a continuum model for scattering of plane elastic waves of arbitrary angle of incidence and polarization from an elastic cylindrical discontinuity in isotropic media. The model fixes several deficiencies that were present in a classic treatise on the subject [1] that enable it to make accurate predictions at oblique angles of incidence.

This manuscript provides insights as to which mechanisms of contrast are responsible for control of the scattering cross section in both the Mie and Rayleigh scattering regimes. In particular we find that in the early Mie regime, scattering efficiency is strongly influenced both elastic and density contrast. While either mechanisms can be used to raise the scattering cross section, there contributions are not always complimentary. In particular, choosing matrix/embedded materials with similar sound speed greatly suppresses scattering cross section in the Mie regime. In the Rayleigh regime, density contrast is found to be the most effective mechanism of scattering contrast for longitudinal waves and for transverse waves polarized perpendicular to the cylinder axis (y-transverse). For quasi-z transverse waves at oblique angles of incidence, elastic and density contrast mechanisms have similar effectiveness.

Thus, the current model predicts the mode-resolved scattering cross section for all acoustic waves in isotropic elastic media with embedded elastic cylinders, over all scattering regimes without resorting to perturbation theory. The model is quite general and can to be applied to a diverse set of engineering applications. In particular, we envision that it will be useful in supporting rapid calculations of the anisotropic thermal conductivity tensor for composites with embedded cylinders using Boltzmann transport theory, which requires mode resolved scattering cross section information at all angle of incidence.

**Acknowledgements**

This material is based upon work supported by the National Science Foundation under Grant No. 1653270. This research was supported in part through the use of the Farber computer cluster and associated Information Technologies (IT) resources at the University of Delaware.

**References**


[1] White, R. M., 1958. "Elastic wave scattering at a cylindrical discontinuity in a solid". *Journal of the Acoustical Society of America,* ***30***(8), pp. 771–785.

[2] Abramowitz, M., and Stegun, I. A., 1964. *Handbook of Mathematical Functions with Formulas, Graphs, and Mathematical Tables*, 9th ed. Dover, New York.

[3] Feser, J. P., 2018. MATLAB software to calculate the scattering cross section of embedded cylinders in isotropic linear elastic media. `https://github.com/jpfeser/CylinderScattering`.

[4] Kakodkar, R. R., and Feser, J. P., 2015. "A framework for solving atomistic phonon-structure scattering problems in the frequency domain using perfectly matched layer boundaries". *Journal of Applied Physics,* ***118***(9).

**List of Figures**



**List of Tables**

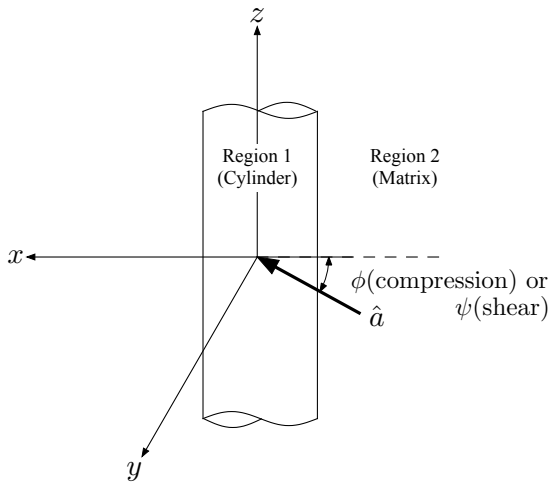


Fig. 1. Coordinate axes and angle definitions for the scattering problem. Vector $\hat{a}$ lies in plane x-z

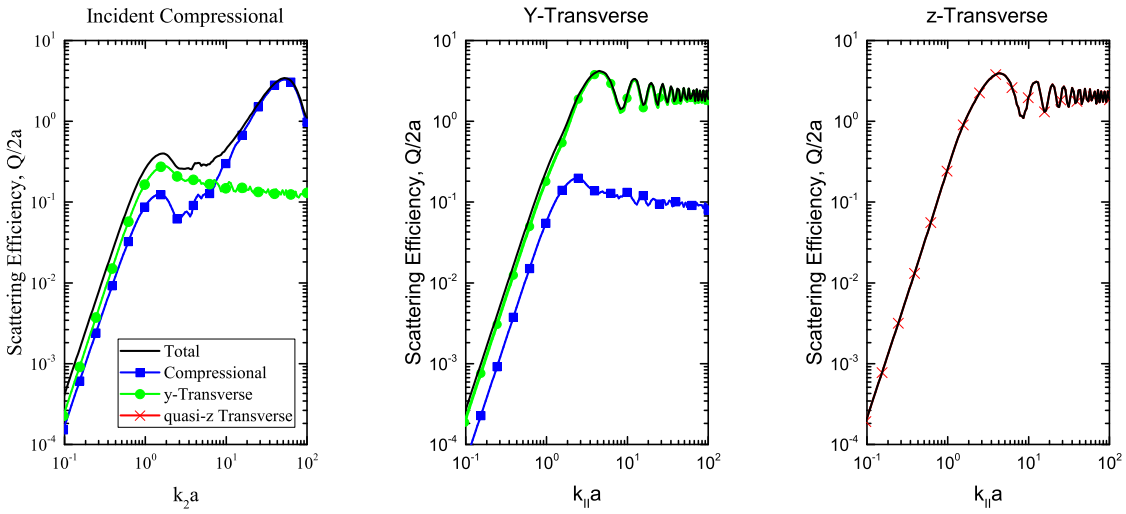


Fig. 2. Scattering efficiency of $NiSi_2$ cylinders in $Si_{0.5}Ge_{0.5}$ as a function of scattering parameter at normal angle-of-incidence for different incident polarizations. Black lines indicate the total scattering scattering efficiency while symbols indicate the portion scattered into compressional (blue box), y-transverse (green circle), and quasi-z transverse modes (red cross).

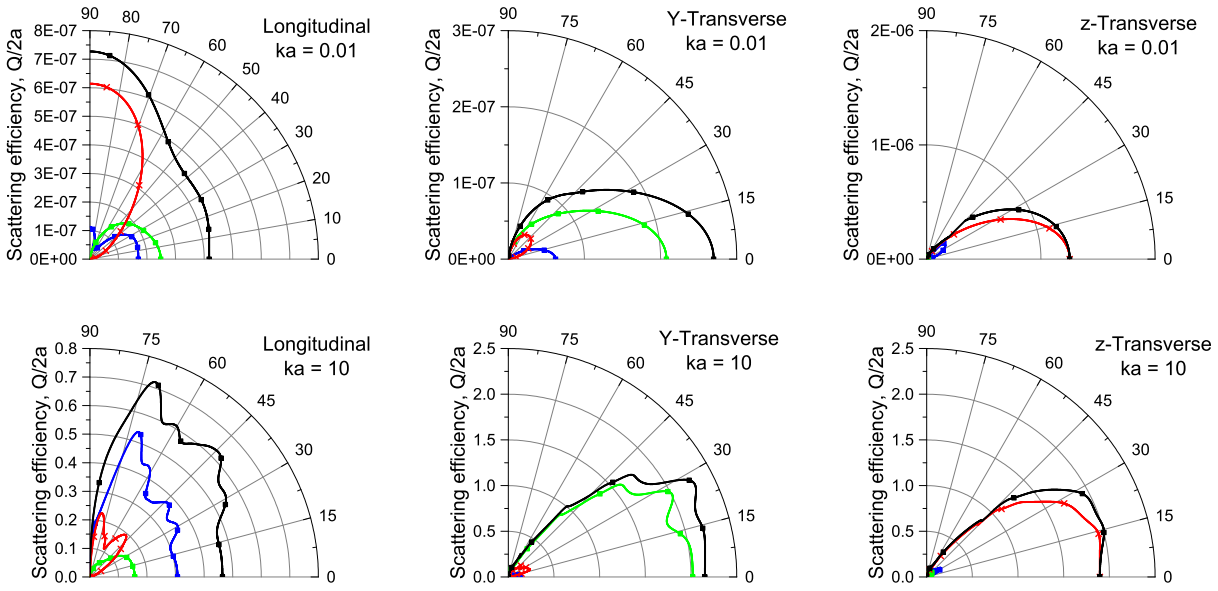


Fig. 3. Scattering efficiency of $NiSi_2$ cylinders in $Si_{0.5}Ge_{0.5}$ as a function of scattering parameter at normal angle-of-incidence for different incident polarizations. Black lines indicate the total scattering scattering efficiency while symbols indicate the portion scattered into compressional (blue box), y-transverse (green circle), and quasi-z transverse modes (red cross).

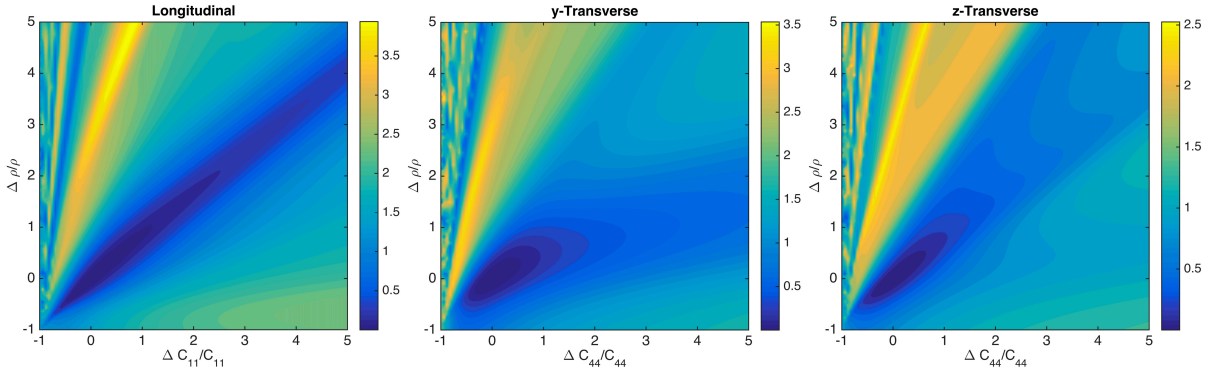


Fig. 4. Scattering efficiency as a function of relative elastic and density contrast in the Mie regime ($ka = 2$) at an oblique angle of incidence, $\phi_2 = 35^\circ$(longitudinal) or $\psi_2 = 35^\circ$(transverse).

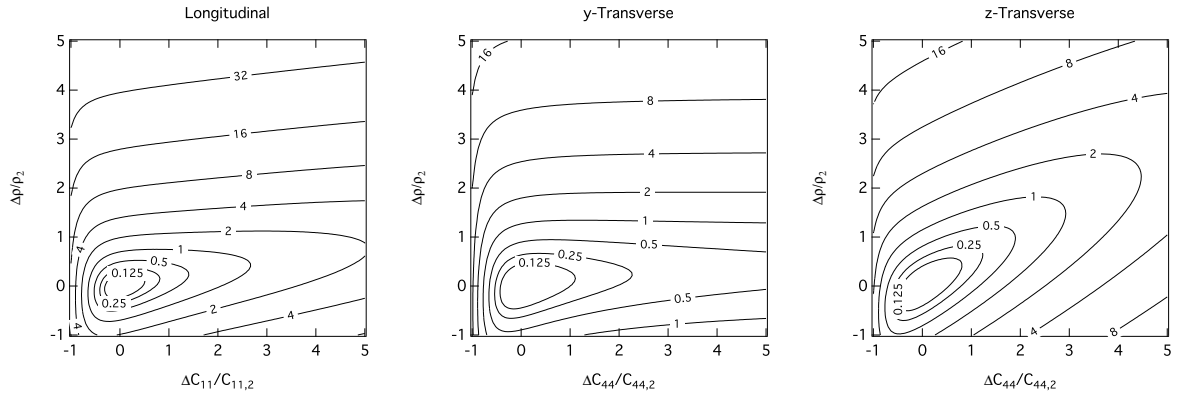


Fig. 5. $\alpha \equiv Q/(2k^3a^4)$ as a function of relative elastic and density contrast in the Rayleigh regime ($ka \ll 1$) at an oblique angle of incidence, $\phi_2 = 35°$(longitudinal) or $\psi_2 = 35°$(transverse).

Table 1. Definition of $\beta_n$ for the three polarizations of incident plane waves.

| Polarization Vector | Mode Name | $\beta_n$ |
|---|---|---|
| $\hat{a}$ | longitudinal | $u_0 e_n i^{n-1}/(k_2)$ |
| $\hat{z} \times \hat{a}$ | y-transverse | $u_0 e_n i^{n-1}/(k_{\mathrm{II}})$ |
| $\hat{z} \times \hat{a} \times \hat{a}$ | quasi-z-transverse | $u_0 e_n i^{n-2}/(k_{\mathrm{II}})$ |

Table 2. Displacement and stress components for an incident longitudinal wave

| Component | Expression |
|---|---|
| $U_r/(1/r)$ | $\sum_{n=0}^{\infty} \beta_n e^{iKz} [-x_2' J_n'(x_2')] \cos(n\theta)$ |
| $U_\theta/(1/r)$ | $\sum_{n=0}^{\infty} \beta_n e^{iKz} [n J_n(x_2')] \sin(n\theta)$ |
| $U_z/(1/r)$ | $\sum_{n=0}^{\infty} \beta_n e^{iKz} [-i(Kr) J_n(x_2')] \cos(n\theta)$ |
| $T_{rr}/(\mu_2/r^2)$ | $\sum_{n=0}^{\infty} \beta_n e^{iKz} \left[-2(x_2')^2 \left(J_n''(x_2') - \left(\frac{x_2}{x_2'}\right)^2 \left(\frac{\lambda_2}{2\mu_2}\right) J_n(x_2')\right)\right] \cos(n\theta)$ |
| $T_{r\theta}/(\mu_2/r^2)$ | $\sum_{n=0}^{\infty} \beta_n e^{iKz} [2n((x_2')J_n'(x_2') - J_n(x_2'))] \sin(n\theta)$ |
| $T_{rz}/(\mu_2/r^2)$ | $\sum_{n=0}^{\infty} \beta_n e^{iKz} [-2i(x_2')(Kr) J_n'(x_2')] \cos(n\theta)$ |

Table 3. Displacement and stress components for a y-transverse incident wave

| Component | Expression |
|---|---|
| $U_r/(1/r)$ | $\sum_{n=0}^{\infty} \beta_n e^{iKz} [-nJ_n(x_{II}')] \cos(n\theta)$ |
| $U_\theta/(1/r)$ | $\sum_{n=0}^{\infty} \beta_n e^{iKz} \left[-\left(k_{II}' r\right) J_n'(x_{II}')\right] \sin(n\theta)$ |
| $U_z/(1/r)$ | $0$ |
| $T_{rr}/(\mu_2/r^2)$ | $\sum_{n=0}^{\infty} \beta_n e^{iKz} [-2n\,(x_{II}' J_n'(x_{II}') - J_n(x_{II}'))] \cos(n\theta)$ |
| $T_{r\theta}/(\mu_2/r^2)$ | $\sum_{n=0}^{\infty} \beta_n e^{iKz} \left[-(x_{II}')^2 (2J_n''(x_{II}') + J_n(x_{II}'))\right] \sin(n\theta)$ |
| $T_{rz}/(\mu_2/r^2)$ | $\sum_{n=0}^{\infty} \beta_n e^{iKz} (Kr) [-inJ_n(x_{II}')] \cos(n\theta)$ |

Table 4. Displacement and stress components for a quasi-z transverse incident wave

| Component | Expression |
|---|---|
| $U_r/(1/r)$ | $\sum_{n=0}^{\infty} \beta_n e^{iKz} \left[ i(Kr) \left( \frac{x_{II'}{}'}{x_{II'}} \right) J_n{}'(x_{II'}{}') \right] \cos(n\theta)$ |
| $U_\theta/(1/r)$ | $\sum_{n=0}^{\infty} \beta_n e^{iKz} \left[ in \left( \frac{Kr}{x_{II'}} \right) J_n(x_{II'}{}') \right] \sin(n\theta)$ |
| $U_z/(1/r)$ | $\sum_{n=0}^{\infty} \beta_n e^{iKz} \left[ \frac{(x_{\mathrm{II}}{}')^2 J_n(x_{\mathrm{II}}{}')}{x_{\mathrm{II}}} \right] \cos(n\theta)$ |
| $T_{rr}/(\mu_2/r^2)$ | $\sum_{n=0}^{\infty} \beta_n e^{iKz} \left[ 2i(x_{\mathrm{II}}{}')^2 \left( \frac{Kr}{x_{\mathrm{II}}} \right) J_n{}''(x_{\mathrm{II}}{}') \right] \cos(n\theta)$ |
| $T_{r\theta}/(\mu_2/r^2)$ | $\sum_{n=0}^{\infty} \beta_n e^{iKz} \left[ 2in \frac{Kr}{x_{\mathrm{II}}} \left( x_{\mathrm{II}}{}' J_n{}'(x_{\mathrm{II}}{}') - J_n(x_{\mathrm{II}}{}') \right) \right] \sin(n\theta)$ |
| $T_{rz}/(\mu_2/r^2)$ | $\sum_{n=0}^{\infty} \beta_n e^{iKz} \left[ \frac{2(x_{\mathrm{II}}{}')^3 J_n{}'(x_{\mathrm{II}}{}')}{x_{\mathrm{II}}} \left( 1 - \frac{1}{2\cos^2\psi_2} \right) \right] \cos(n\theta)$ |

Table 5. To obtain the scattered wave field in region 1, the following substitutions are needed in Eqs. 15-21.

| Region 2 | Region 1 |
|---|---|
| $A_n$ | $D_n$ |
| $B_n$ | $E_n$ |
| $C_n$ | $F_n$ |
| $H_n(z)$ | $J_n(z)$ |
| Subscript 2 | Subscript 1 |
| Subscript II | Subscript I |

Table 6. Displacement and Stress Tensor Components associated with scattered wave $L_2$; to obtain the analogous expressions in medium 1, make the substitutions in Table 5

| Component | Expression |
|---|---|
| $\frac{(U_r)_{L_2}}{(1/a)}$ | $\sum_{n=0}^{\infty} A_n e^{iKz}\left[-x_2' H_n'(x_2')\right] \begin{matrix}\cos(n\theta)\\ \sin(n\theta)\end{matrix}$ |
| $\frac{(U_\theta)_{L_2}}{(1/a)}$ | $\sum_{n=0}^{\infty} A_n e^{iKz}\left[\pm n H_n(x_2')\right] \begin{matrix}\sin(n\theta)\\ \cos(n\theta)\end{matrix}$ |
| $\frac{(U_z)_{L_2}}{(1/a)}$ | $\sum_{n=0}^{\infty} A_n e^{iKz}\left[-i(Kr) H_n(x_2')\right] \begin{matrix}\cos(n\theta)\\ \sin(n\theta)\end{matrix}$ |
| $\frac{(T_{rr})_{L_2}}{(\mu_2/a^2)}$ | $\sum_{n=0}^{\infty} A_n e^{iKz}\left[-2(x_2')^2\left(H_n''(x_2') - \left(\frac{x_2}{x_2'}\right)^2\left(\frac{\lambda_2}{2\mu_2}\right) H_n(x_2')\right)\right] \begin{matrix}\cos(n\theta)\\ \sin(n\theta)\end{matrix}$ |
| $\frac{(T_{r\theta})_{L_2}}{(\mu_2/a^2)}$ | $\sum_{n=0}^{\infty} A_n e^{iKz}\left[\pm 2n\left((x_2')H_n'(x_2') - H_n(x_2')\right)\right] \begin{matrix}\sin(n\theta)\\ \cos(n\theta)\end{matrix}$ |
| $\frac{(T_{rz})_{L_2}}{(\mu_2/a^2)}$ | $\sum_{n=0}^{\infty} A_n e^{iKz}\left[-2i(x_2')(Kr) H_n'(x_2')\right] \begin{matrix}\cos(n\theta)\\ \sin(n\theta)\end{matrix}$ |

Table 7. Displacement and Stress Tensor Components associated with scattered wave $M_2$; to obtain the analogous expressions in medium 1, make the substitutions in Table 5

| Component | Expression |
|---|---|
| $\frac{(U_r)_{M_2}}{(1/a)}$ | $\sum_{n=0}^{\infty} B_n e^{iKz}(\pm nH_n\left(k_{II}{}'r\right))\begin{matrix}\cos(n\theta)\\ \sin(n\theta)\end{matrix}$ |
| $\frac{(U_\theta)_{M_2}}{(1/a)}$ | $\sum_{n=0}^{\infty} B_n e^{iKz}(-\left(k_{II}{}'r\right)H_n{}'\left(k_{II}{}'r\right))\begin{matrix}\sin(n\theta)\\ \cos(n\theta)\end{matrix}$ |
| $\frac{(U_z)_{M_2}}{(1/a)}$ | $0$ |
| $\frac{(T_{rr})_{M_2}}{(\mu_2/a^2)}$ | $\sum_{n=0}^{\infty} B_n e^{iKz}[\pm 2n\left(x_{II}{}'H_n{}'\left(x_{II}{}'\right)-H_n\left(x_{II}{}'\right)\right)]\begin{matrix}\cos(n\theta)\\ \sin(n\theta)\end{matrix}$ |
| $\frac{(T_{r\theta})_{M_2}}{(\mu_2/a^2)}$ | $\sum_{n=0}^{\infty} B_n e^{iKz}\left[-\left(x_{II}{}'\right)^2\left(2H_n{}''\left(x_{II}{}'\right)+H_n\left(x_{II}{}'\right)\right)\right]\begin{matrix}\sin(n\theta)\\ \cos(n\theta)\end{matrix}$ |
| $\frac{(T_{rz})_{M_2}}{(\mu_2/a^2)}$ | $\sum_{n=0}^{\infty} B_n e^{iKz}\left(Kr\right)[\pm inH_n(x_{II}{}')]\begin{matrix}\cos(n\theta)\\ \sin(n\theta)\end{matrix}$ |

Table 8. Displacement and Stress Tensor Components associated with scattered wave $N_2$; to obtain the analogous expressions in medium 1, make the substitutions in Table 5

| Component | Expression |
|---|---|
| $\frac{(U_r)_{N_2}}{(1/a)}$ | $\sum_{n=0}^{\infty} C_n e^{iKz}\left[i(Kr)\left(\frac{x_{II}{}'}{x_{II}}\right)H_n{}'(x_{II}{}')\right]\begin{matrix}\cos(n\theta)\\ \sin(n\theta)\end{matrix}$ |
| $\frac{(U_\theta)_{N_2}}{(1/a)}$ | $\sum_{n=0}^{\infty} C_n e^{iKz}\left[\mp in\left(\frac{Kr}{x_{II}}\right)H_n(x_{II}{}')\right]\begin{matrix}\sin(n\theta)\\ \cos(n\theta)\end{matrix}$ |
| $\frac{(U_z)_{N_2}}{(1/a)}$ | $\sum_{n=0}^{\infty} C_n e^{iKz}\left[\left(\frac{(x_{II}{}')^2}{x_{II}}\right)H_n(x_{II}{}')\right]\begin{matrix}\cos(n\theta)\\ \sin(n\theta)\end{matrix}$ |
| $\frac{(T_{rr})_{N_2}}{(\mu_2/a^2)}$ | $\sum_{n=0}^{\infty} C_n e^{iKz}\left[2i(x_{II}{}')^2\left(\frac{Kr}{x_{II}}\right)H_n{}''(x_{II}{}')\right]\begin{matrix}\cos(n\theta)\\ \sin(n\theta)\end{matrix}$ |
| $\frac{(T_{r\theta})_{N_2}}{(\mu_2/a^2)}$ | $\sum_{n=0}^{\infty} C_n e^{iKz}\left[\mp 2in\frac{Kr}{x_{II}}\left(x_{II}{}'H_n{}'(x_{II}{}')-H_n(x_{II}{}')\right)\right]\begin{matrix}\sin(n\theta)\\ \cos(n\theta)\end{matrix}$ |
| $\frac{(T_{rz})_{N_2}}{(\mu_2/a^2)}$ | $\sum_{n=0}^{\infty} C_n e^{iKz}\left[\frac{2(x_{II}{}')^3H_n{}'(x_{II}{}')}{x_{II}}\left(1-\frac{1}{2\cos^2\psi_2}\right)\right]\begin{matrix}\cos(n\theta)\\ \sin(n\theta)\end{matrix}$ |

Table 9. Parameters used to generate figures 2 and 3

| Parameter | $Si_{0.5}Ge_{0.5}$ | $NiSi_2$ |
|---|---|---|
| $\rho$ [kg/m$^3$] | 3826 | 4803 |
| $C_{11}$ [GPa] | 146 | 199 |
| $C_{44}$ [GPa] | 74 | 53 |